Journal of African Earth Sciences 102 (2015) 102–115

Contents lists available at ScienceDirect

Journal of African Earth Sciences

journal homepage: www.elsevier.com/locate/jafrearsci

Petrogenesis of carbonated meta-ultramafic lenses from the Neoproterozoic Heiani ophiolite, South Eastern Desert, Egypt: A natural analogue to CO_2 sequestration

Hisham A. Gahlan [a,*], Shoji Arai [b], Sattam A. Almadani [a]

[a] Department of Geology and Geophysics, King Saud University, Riyadh 11451, Saudi Arabia
[b] Department of Earth Sciences, Kanazawa University, Kanazawa 920-1192, Japan

ARTICLE INFO

Article history:
Received 29 March 2014
Received in revised form 23 July 2014
Accepted 5 November 2014
Available online 23 November 2014

Keywords:
Meta-ultramafic
Carbonate-orthopyroxenite
Low-*P*/high-*T* regional metamorphism
CO_2-metasomatism
Heiani ophiolite

ABSTRACT

Among a set of peculiar meta-ultramafics, carbonate-orthopyroxenites are observed for the first time in the Heiani ophiolite belt, South Eastern Desert, Egypt. They form massive lensoidal masses up to 50 m long and 20 m wide. The lenses show a marked structural concordance with their neighboring country rocks. The typical country rocks are represented by the following high-grade metamorphic rocks: kyanite–muscovite schists, amphibolites, kyanite-bearing biotite gneisses, migmatites, granite gneisses and mobilizates. The studied carbonate-orthopyroxenites consist mainly of metamorphic orthopyroxene + magnesite, among other metamorphic, relict primary and retrograde secondary minerals. According to primary chromian spinel (Cr#, 0.7–0.84) chemistry and morphology, absence of clinopyroxene and presence of primary mantle olivine ($Fo_{89–91}$) as relicts in the metamorphic orthopyroxene, the Heiani carbonate-orthopyroxenites seem to have formed from a highly depleted mantle peridotite precursor. At a late collisional stage during the Pan-Africa terrane accretion and the E–W crustal shortening (ca. 650–620 Ma), high-grade (upper amphibolite facies) low-*P*/high-*T* regional metamorphism (ca. 660 Ma) accompanied by CO_2-metasomatism resulted in formation of the Heiani carbonate-orthopyroxenites. Mostly the carbonate-bearing shelf sediments beneath and/or in juxtaposition with the Heiani ophiolite are considered to be the proven source of the CO_2-rich fluids. Although, a mixed sedimentary-mantle C source is not unlikely. A mineral paragenetic correlation with experimental data for the system MgO–SiO_2–H_2O–CO_2 suggests metamorphic conditions consistent with those of the high-grade country rocks; i.e. 630–650 °C, 6–7 kbar (20–23 km depth) and high-X_{CO2} (0.6–0.7). The CO_2-bearing fluids discharging along faults gave rise to regionally widespread carbonate-bearing assemblages. Accordingly, the Heiani carbonate-orthopyroxenites are considered the by-products of natural carbon sequestration by an ultramafic rock.

1. Introduction

The carbonate-bearing meta-ultramafics and listvenites (*sensu stricto*) are results of various degrees of carbonatization and/or silicification (e.g. Halls and Zhao, 1995; Akbulut et al., 2006 and references therein). They represent a natural analogue to CO_2 sequestration via *in situ* mineral carbonation that has the ability to fix anthropogenic CO_2 (e.g. Seifritz, 1990; Hansen et al., 2005). Accordingly, they have attracted attention from either scientific or applied perspective.

A conspicuous meta-ultramafic rock consisting mainly of orthopyroxene and magnesite in the Caledonian mountain belt, near the Lake Sagvandet, Troms, Norway, has been found and named *sagvandite* by Pettersen (1883). In the Lyngenfjord area, 60 km north of the Lake Sagvandet, Reitan and Geul (1958) and Randall (1960) recorded a sagvandite-like rock (orthopyroxene + dolomite). Evans and Trommsdorff (1974) recorded a similar rock in the metaperidotites of Val D'efra, Lepontine Alps, and named it MEFT (magnesite–enstatite–forsterite–talc rock). In the Gerf ophiolite, South Eastern Desert, Egypt, Gahlan and Arai (2009) recorded the classic sagvandite rock, and treated them under the term carbonate-orthopyroxenite.

Origin of the above mentioned meta-ultramafics has been a matter of debate, and a variety of origins have been proposed for these rocks: sedimentary (e.g. Pettersen, 1883; Rosenbusch, 1884), magmatic (e.g. Barth, 1926), metamorphic differentiation and/or metasomatism of carbonate-rich sediments (e.g. Reitan

* Corresponding author. Tel.: +966 1146 76211; fax: +966 1146 76214.
E-mail address: hjhlan@yahoo.com (H.A. Gahlan).

http://dx.doi.org/10.1016/j.jafrearsci.2014.11.002
1464-343X/

and Geul, 1958; Randall, 1960), regional metamorphism accompanied by CO_2-metasomatism of ultramafics (e.g. Schreyer et al., 1972; Evans and Trommsdorff, 1974), and/or thermal metamorphism accompanied by CO_2-metasomatism of ultramafics (e.g. Gahlan and Arai, 2009).

We discovered *classic sagvandite* within the Neoproterozoic Heiani ophiolite, South Eastern Desert (SED), Egypt. As far as we know, such rocks are very rare in the Pan-African Proterozoic ophiolites (Gahlan, 2006; Gahlan and Arai, 2009). To eliminate ambiguity of the term *sagvandite*, we will use the term carbonate-orthopyroxenite for the studied rocks (e.g. Schreyer et al., 1972; Gahlan and Arai, 2009). In spite of the great similarities in protolith and tectonic setting, the Heiani carbonate-orthopyroxenites cannot be regarded as listvenites (*sensu stricto*) (for more details see Halls and Zhao, 1995).

Based on detailed field work, petrography and mineral chemistry, this contribution provides an overview of origin and petrology of the Heiani carbonate-orthopyroxenites. In addition, we shed some light on the mechanism of formation of this rock type during the Pan-African orogeny.

2. Geological outline

The Heiani district (the eastern portion of the Allaqi-Heiani ophiolite belt) lies in the extreme southern part of the South Eastern Desert (SED) of Egypt (Fig. 1), about 111 km southwest of Shalatin City. The Allaqi-Heiani ophiolite-decorated fold and thrust belt extends for more than 250 km from the N–S-trending Hamisana Shear Zone (HSZ) in the east till Nasser Lake in the west (Fig. 1). The Allaqi-Heiani ophiolite belt (ca. 800–730 Ma; Kröner et al., 1992; Ali et al., 2010) is the westernmost part of the famous Yanbu–Onib–Sol-Hamed–Gerf–Allaqi-Heiani (YOSHGAH) suture (e.g. Ren and Abdelsalam, 2006). It is the northernmost arc–arc suture in the Arabian Nubian Shield (ANS) that separates the Egyptian SED terrane (ca. 750 Ma) in the north from the Sudanese Gabgaba terrane to the south (ca. 830–720 Ma) (e.g. Kröner et al., 1987; Abdelsalam and Stern, 1996; Ali et al., 2010).

The YOSHGAH was a coherent contiguous ophiolite nappe that was dextrally displaced by the N-trending HSZ (640–600 Ma) (Stern et al., 1989, 1990; de Wall et al., 2001). The Allaqi-Heiani ophiolite belt changes its orientation from N-trending along the HSZ to E–W-trending farther west beyond limits of the map area (Fig. 1). The included part of the Allaqi-Heiani ophiolite belt in the map area, the Heiani ophiolite, is about 25 km long from its eastern end along the HSZ (Figs. 1 and 2).

The area under investigation (Fig. 2) is a folded thrust belt, and can be described in terms of four main lithotectonic units: basal gneisses, ophiolite, island-arc assemblage and late- to post-tectonic granites (e.g., Kröner et al., 1987; Greiling et al., 1994; Abdelsalam et al., 2003; Zoheir and Klemm, 2007; Abdeen and Abdelghaffar, 2011). The autochthonous gneisses and migmatites (Tier I of Greiling et al., 1994) (ca. 660 Ma; Stern et al., 1989) have been overthrust by allochthonous molasse-facies sedimentary and ophiolitic nappes (Tier II of Greiling et al., 1994). The ophiolitic rocks are tectonically topping the nappe pile, with an original thrusting direction toward the south and southwest (e.g. Kröner et al., 1987; Stern et al., 1990; Gahlan, 2006; Zoheir and Klemm, 2007). Subsequently, the whole structural sequence, Tires I and II, has been intruded by late- to post-tectonic granites (~650–510 Ma; Stern et al., 1989; Moussa et al., 2008).

The Heiani ophiolite nappe comprises a tectonic mélange of highly deformed ophiolitic assemblage, shelf metasediments, arc volcanics and volcaniclastics. It forms a large NW–SE-trending asymmetrical synform (Fig. 2), with an axial plane dipping steeply (55–65°) to the NE (i.e. SW-verging). Close to the HSZ, the

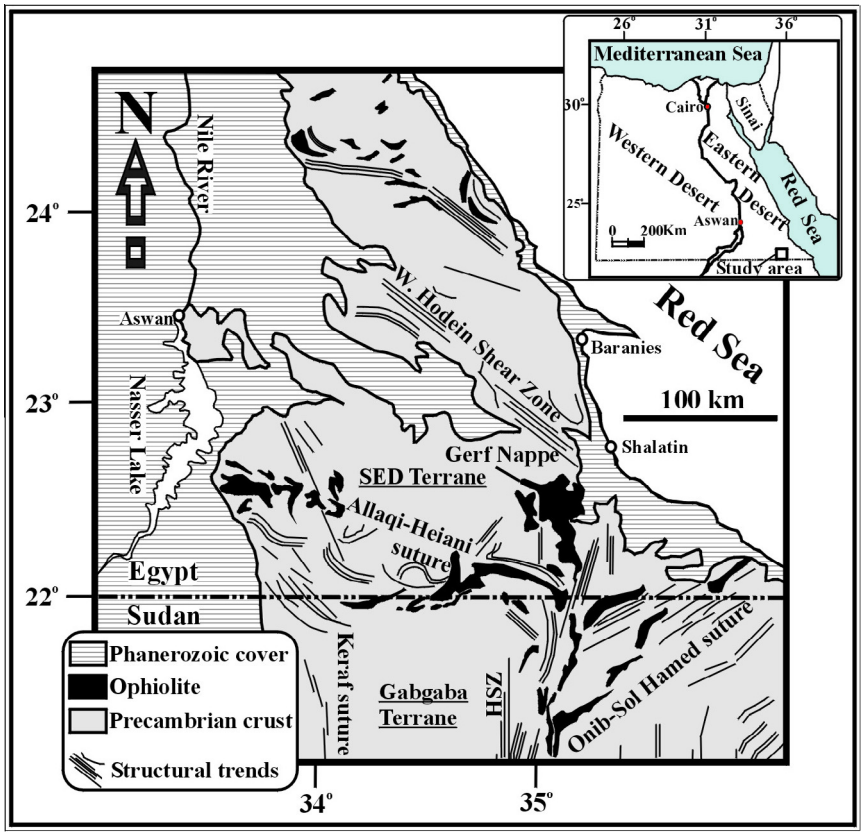

Fig. 1. The Allaqi-Heiani suture within the South Eastern Desert (SED) of Egypt and northeastern Sudan (modified after Ramadan et al., 2001). HSZ, Hamisana Shear Zone.

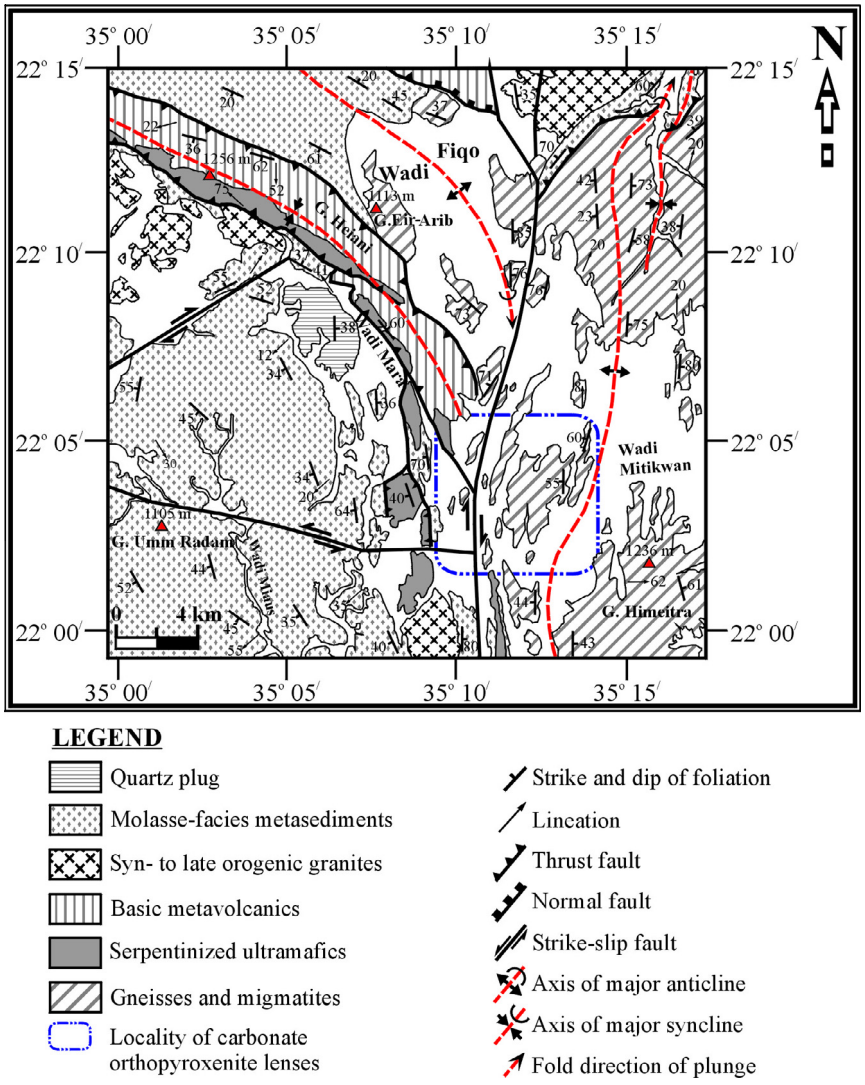

Fig. 2. Geological and structural map of the Heiani ophiolite (modified after Gahlan, 2006) showing filed relations around the carbonate-orthopyroxenite locality.

SW-verging folds and thrust sheets have been deformed and overprinted by N-trending folds and shear zones pertaining to the HSZ (Fig. 2).

According to the Penrose Conference (Anonymous, 1972), the Heiani ophiolite is moderately dismembered and offers imbricated thrust sheets/lenses of the mantle section, gabbroic crust and mafic volcanics. Contacts between members of the Heiani ophiolite, although initially magmatic/stratigraphic, are modified by tectonism to be structural (low-angle thrust faults). The Heiani mantle section is represented by, mappable, massive lenses and sheet-like bodies of serpentinites, carbonatized metaperidotites and talc-carbonate schists. The latter lithologies occur mostly on one horizon, being preserved in the trough of G. Heiani major synform, and are concordantly incorporated into basic metavolcanics (Fig. 2). The Heiani mantle section is dominated by totally serpentinized harzburgite (opx bastite ~10 vol.%) with less abundant concordant serpentinized dunite lenses, bands and veins. We observed concordant small-scale chromitite pods (⩽4 m long) being enveloped by serpentinized dunite, and both are collectively enclosed by serpentinized harzburgite. The Heiani gabbroic crust and mafic volcanic carapace are metamorphosed to various extents, being represented by intervening amphibolite mega shear pods.

Among a set of peculiar metaperidotites, carbonate-orthopyroxenites (sagvandites; Pettersen, 1883) are observed on the intersection between Wadi Fiqo and Wadi Mitikwan, mainly along the HSZ (Fig. 2). They form rootless lensoidal masses (up to 50 m long and 20 m wide) striking N–S to NNE–SSW and dipping by 40° toward W (Fig. 3A and B). The Heiani carbonate-orthopyroxenites show a marked concordance with the plano-linear fabrics of the metamorphic country rocks and major shear zones (Fig. 3A and B). The country rocks show a typical metamorphic foreland association (e.g., El Gaby et al., 1988); namely: garnet–cordierite–kyanite–biotite gneisses and migmatites, amphibolites, kyanite–quartz veins, cordierite aploids, and marbles (Gahlan, 2006). Notably, the carbonatization of ultramafics becomes more extensive close to marble and impure carbonate layers within the metasedimentary country rocks. As well as, close to shear zones and thrust faults. Along peripheries of the Heiani carbonate-orthopyroxenites, neither chilled margins, reaction haloes nor xenoliths from the country rocks are observed. Based on the above mentioned field relations, large similarities have been observed between the Heiani carbonate-orthopyroxenites and their counterpart in the type locality, Troms, Norway (Schreyer et al., 1972).

Megascopically, the carbonate-orthopyroxenites are coarse-grained, massive and/or pseudoporphyritic (Fig. 3C). Moreover,

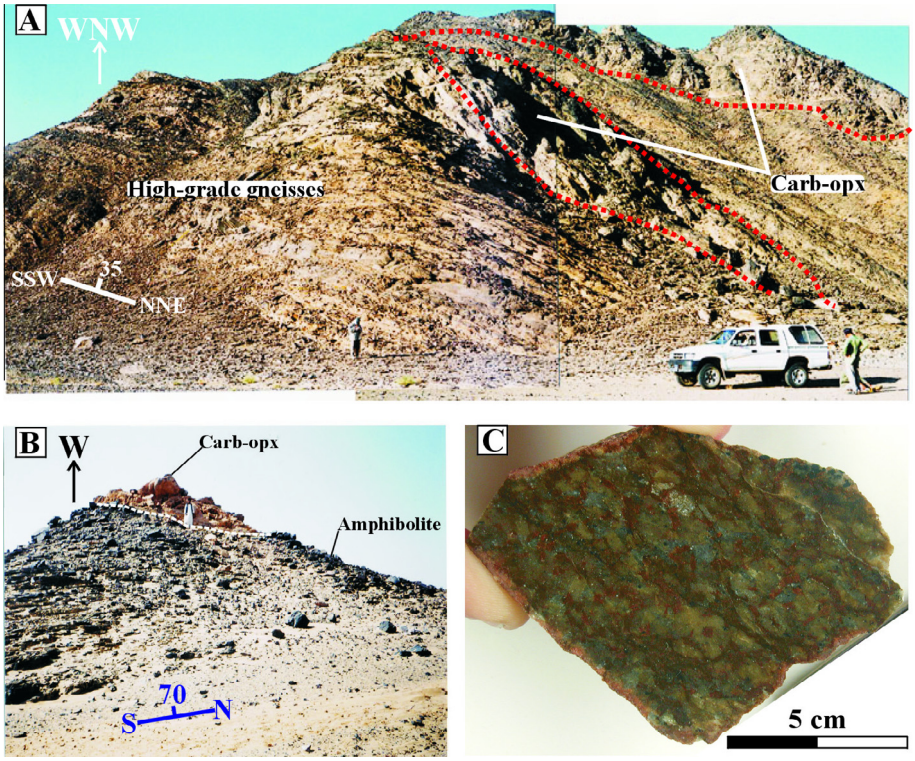

Fig. 3. Selected field photographs of carbonate-orthopyroxenites from the Heiani ophiolite, SED, Egypt. (A) Carbonate-orthopyroxenite lenses concordantly overlies (and/or being incorporated into) the foliated high-grade gneisses; East of the HSZ, foliation: 296/35°. (B) Steeply-dipping, N–S- to NNE–SSW-striking, rootless, massive lensoidal carbonate-orthopyroxenites along the HSZ. (C) Close-up view of a sawed surface of carbonate-orthopyroxenite.

they show characteristic salmon-pink or rusty red[1] weathered surfaces (Fig. 3C) that can be attributed to subsequent supergene weathering, where iron is released from breunnerite to form iron oxides (e.g. Halls and Zhao, 1995). Orthopyroxene and olivine crystals are commonly floating in a conspicuous pink-colored carbonate groundmass (Fig. 3C). Moreover, cross-cutting pink-colored carbonate veinlets are widespread.

3. Petrography

Based on the most prominent and characteristic rock-forming minerals, the metaperidotites (described herein) are named carbonate-orthopyroxenites. The latter nomenclature has been adopted from Schreyer et al. (1972). Microscopically, they consist mainly of orthopyroxene (40–60% by volume), carbonate (40–55% by volume) and olivine (0–10% by volume), with an occasional predominance of carbonate over silicates. Accessories are spinel and pentlandite. Retrograde alteration products are represented by talc, serpentine and magnetite. Notably, no sign of protolith texture has been observed (Fig. 4). The Heiani carbonate-orthopyroxenites are overall similar in texture and mineral assemblage to their counterpart in the type locality, Troms, Norway (Schreyer et al., 1972), except for their lower orthopyroxene/carbonate ratio and the absence of phlogopite. Compared with the Gerf carbonate-orthopyroxenites (Gahlan and Arai, 2009), those of the Heiani are characterized by absence of the anthophyllite, tremolite, chlorite, ferritchromite and Cr-magnetite.

The orthopyroxene (0.5–40 mm long) forms idioblastic, long prismatic, homogeneous porphyroblasts, with no exsolution lamellae of clinopyroxene (Fig. 4A). Occasionally, orthopyroxenes replace olivine relics during prograde metamorphism (Fig. 4A and B). The olivine (0.1–2 mm across) forms anhedral to subhedral crystals, being free from opaque minute inclusions (Fig. 4A and B). During retrograde metamorphism, olivine is replaced by magnesite, talc and serpentine (Fig. 4B and C). Carbonates are mostly magnesite (up to 10 mm across) that forms anhedral to subhedral, rhombohedral or polygonal crystals, as well as crystal clusters and veinlets. They commonly constitute the groundmass, displaying a well-developed granoblastic polygonal mosaic texture (Fig. 4C). Talc (0.1–1 mm long) forms flakes, fine crystalline aggregates, as well as clusters (Fig. 4C) that commonly replace orthopyroxene and olivine along grain boundaries and cracks (Fig. 4C). Pseudomorphs after orthopyroxene being completely made up by talc are observed. Serpentine is the most common retrograde alteration product, and forms either chrysotile cross-fiber veinlets or lizardite interstitial between the major constituents. Chrysotile constitutes the common mesh texture after olivine, and lizardite constitutes the bastite texture after orthopyroxene (Fig. 4D).

Chromian spinel ($\leqslant$2% by volume) ($\leqslant$1 mm across) forms euhedral to subhedral crystals, with reddish brown and dark gray colors respectively in transmitted and reflected lights. It is commonly scattered within the groundmass or is included in orthopyroxene, magnesite and/or primary olivine (Fig. 4A and B). Neither optical nor chemical zonation has been observed. Magnetite forms anhedral to ragged crystals ($\leqslant$1 mm across) or fine dust. Octahedral magnetite crystals that yield triangular or rhombic sections are not uncommon. It shows several modes of occurrences such as random scattering, fracture-filling, and inclusions in metamorphic and/or retrograde mineral phases (Fig. 4D).

4. Analytical techniques

Minerals on polished thin sections were analyzed by a wavelength dispersive microprobe (JEOL Superprobe JXA-8800R) at

[1] For interpretation of color in Fig. 3, the reader is referred to the web version of this article.

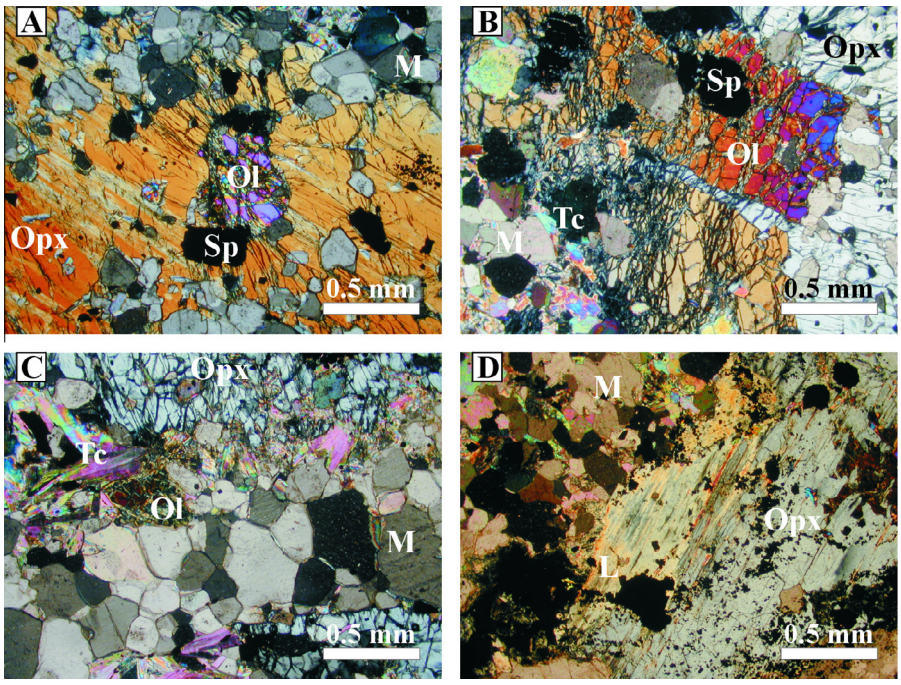

Fig. 4. Photomicrographs of carbonate-orthopyroxenites from the Heiani ophiolite, SED, Egypt. Abbreviations: Ol, olivine; M, magnesite; Opx, orthopyroxene; Tc, talc; Sp, chromian spinel. (A) Poikiloblastic metamorphic orthopyroxene includes, in optical continuity, primary olivine relics and euhedral chromian spinel. Most of the field of view is occupied by a centimeter-sized orthopyroxene crystal. (B) Metamorphic orthopyroxene replaces primary olivine. Note the assemblage (olivine, metamorphic orthopyroxene and magnesite) that defines reaction boundary of the carbonate-orthopyroxenite rocks. (C) Granoblastic polygonal mosaic groundmass consists mainly of magnesite (homeoblastic type texture) with 120° grain-boundary interfacial angle. Note the olivine constituting center of the mesh texture and orthopyroxene being marginally replaced by talc. (D) Pseudoporphyritic metamorphic orthopyroxene, being marginally replaced by lizardite, sets in a granoblastic mosaic groundmass of magnesite.

the Kanazawa University, Japan. The adopted analytical conditions were: 15 kV for accelerating voltage, 20 nA for beam current, and 3 μm for beam diameter with counting times 20 s for major elements and 30–50 s for minor ones. Various natural and synthetic standards have been used. Raw intensities for each element were corrected by the ZAF method, and weight percent of oxides were calculated. All iron in silicates and carbonates was assumed to be ferrous. Ti was assumed to be present in spinel as an ulvöspinel molecule. Fe^{3+} and Fe^{2+} in spinel phases were calculated assuming spinel stoichiometry. Mg# and Cr# are $Mg/(Mg + Fe^{2+})$ and $Cr/(Cr + Al)$ atomic ratios, respectively. Y_{Cr}, Y_{Al} and Y_{Fe} are respectively atomic ratios of Cr, Al and Fe^{3+} to $\sum(Cr + Al + Fe^{3+})$. Representative microprobe analyses of chromian spinel, and silicates and carbonates are summarized, respectively, in Tables 1 and 2.

Trace-element abundances in orthopyroxene (enstatite) were determined *in situ* by a laser ablation system (GeoLas Q-Plus, Microlas) coupled to an ICP-MS system (Agilent 7500_S, Yokogawa Analytical System) at the Kanazawa University (Table 3). Details of the analytical procedure are given in Ishida et al. (2004) and Morishita et al. (2005). The laser-spot diameter was 60 μm at 5 Hz with energy density of 8 J/cm^2 per pulse. The primary calibration standard was NIST SRM 612 glass, with selected element concentrations from the preferred values of Pearce et al. (1997). The standard was analyzed at the beginning of each batch of <3–4 unknowns, with a linear drift correction applied between each calibration. The raw data were quantified by using the SiO_2 contents (determined by EPMA) as an internal standard, following a protocol essentially identical to that outlined by Longerich et al. (1996).

5. Mineral chemistry

The analyzed mineral phases are homogeneous in composition within each sample, although, sample-to-sample chemical heterogeneity is not uncommon.

5.1. Chromian spinels

Relicts of primary spinel, based partly on petrography, are mostly homogenous, with almost no core–rim compositional zoning. They contain 48–55 wt.% Cr_2O_3 and 7–14 wt.% Al_2O_3, corresponding to high and restricted Cr# (0.70–0.84) (Fig. 5; Table 1). Their Mg# (0.26–0.4) is also highly restricted and shows a negative correlation with FeO* (Fig. 5). The Y_{Fe} is lower than 0.09 (mostly around 0.05) (Table 1). TiO_2, MnO and NiO are generally very low, 0.06, 0.2 and 0.03 wt.%, on average, respectively (Table 1). Notably, ferritchromite and Cr-magnetite have never been observed either as discrete grains or as rims developed along grain boundaries and cracks of relict primary spinels.

5.2. Silicates and carbonates

The olivine is compositionally uniform ($Fo_{89–91}$; mostly around Fo_{90}) (Fig. 6; Table 2). Detailed profiling yielded no significant core–rim compositional zoning. The NiO (0.23–0.36 wt.%) and MnO (⩽0.13 wt.%) show no systematic relationship with Mg# in olivine (Fig. 6; Table 2). The concentration of CaO (⩽0.02 wt.%) is close to detection limit of the microprobe (Table 2). The orthopyroxene is enstatite (Mg#, 0.87–0.92). Compared with the enstatite Mg# of the Gerf carbonate-orthopyroxenites (Gahlan and Arai, 2009), that of the Heiani is different (Fig. 7). The Heiani enstatite is characterized by conspicuous depletion in CaO, Al_2O_3 and Cr_2O_3 (Fig. 7; Table 2). Neither chemical zonation nor exsolution lamellae of Ca-rich pyroxene was observed. Apparent Mg–Fe^{2+} partition coefficients between coexisting olivine and orthopyroxene, K_D $(X_{Mg}\ (ol) \cdot X_{Fe}\ (opx)/(X_{Fe}\ (ol) \cdot X_{Mg}\ (opx))$, usually deviate from unity (K_D, 0.8–1.2) (Fig. 8). These K_D values are in contrast with olivine–orthopyroxene pairs from alpine-type peridotites and peridotite nodules (e.g. White, 1966; Peters, 1968; Loney et al., 1971).

Table 1
Representative microprobe analyses (wt.%) of chromian spinel from the Heiani carbonate-orthopyroxenites.

Lithology	Carbonate-orthopyroxenite									
Mineral	Primary chromian spinel									
SiO_2	n.d.	n.d.	n.d.	0.02	0.02	0.03	n.d.	n.d.	n.d.	n.d.
TiO_2	0.04	0.13	0.08	0.03	0.08	0.07	0.10	0.07	0.14	0.06
Al_2O_3	13.09	12.88	12.25	11.26	13.60	11.29	7.87	13.68	6.84	14.56
Cr_2O_3	49.39	52.80	54.82	55.06	51.51	54.69	52.70	55.10	54.05	50.04
FeO	22.30	22.74	22.28	22.52	23.68	23.30	25.22	23.01	24.91	21.89
Fe_2O_3	7.33	3.87	2.29	3.08	4.03	3.19	7.33	0.94	7.35	5.17
MnO	0.15	0.21	0.16	0.23	0.22	0.22	0.24	0.23	0.24	0.20
MgO	7.50	7.21	7.47	7.16	6.64	6.68	4.96	7.19	5.06	7.94
CaO	n.d.	n.d.	0.01	n.d.	n.d.	0.01	n.d.	n.d.	n.d.	n.d.
Na_2O	0.02	n.d.	n.d.	0.02	0.02	n.d.	0.02	n.d.	0.01	0.02
K_2O	0.09	0.13	n.d.	n.d.	0.14	n.d.	n.d.	n.d.	n.d.	0.07
NiO	0.09	0.05	0.02	0.03	0.06	0.01	0.01	0.01	0.02	0.05
Total	100.00	100.00	99.96	100.23	100.00	100.35	100.13	100.60	100.40	100.00
No. of ions on the basis of 4 (O)										
Si	0.000	0.000	0.000	0.001	0.001	0.001	0.000	0.000	0.000	0.000
Ti	0.001	0.003	0.002	0.001	0.002	0.002	0.003	0.002	0.004	0.002
Al	0.510	0.505	0.483	0.447	0.533	0.449	0.324	0.534	0.283	0.563
Cr	1.292	1.388	1.450	1.465	1.355	1.459	1.457	1.442	1.497	1.298
Fe^{2+}	0.628	0.643	0.628	0.639	0.669	0.663	0.741	0.645	0.736	0.611
Fe^{3+}	0.191	0.097	0.060	0.082	0.102	0.084	0.211	0.018	0.210	0.132
Mn	0.004	0.006	0.005	0.007	0.006	0.006	0.007	0.007	0.007	0.006
Mg	0.370	0.357	0.372	0.359	0.329	0.336	0.258	0.355	0.264	0.388
Ca	0.000	0.000	0.001	0.000	0.000	0.000	0.000	0.000	0.000	0.000
Na	0.002	0.000	0.000	0.002	0.002	0.000	0.001	0.000	0.000	0.001
K	0.000	0.000	0.000	0.000	0.000	0.000	0.000	0.000	0.000	0.000
Ni	0.002	0.001	0.001	0.001	0.002	0.000	0.000	0.000	0.001	0.001
Total	3.001	3.000	3.001	3.002	3.000	3.001	3.002	3.002	3.002	3.001
Mg#	0.37	0.36	0.37	0.36	0.33	0.34	0.26	0.35	0.27	0.39
Cr#	0.72	0.73	0.75	0.77	0.72	0.76	0.82	0.73	0.84	0.70
Y_{Cr}	0.65	0.70	0.73	0.74	0.68	0.73	0.74	0.72	0.76	0.65
Y_{Al}	0.26	0.25	0.24	0.22	0.27	0.23	0.16	0.27	0.14	0.28
Y_{Fe}	0.09	0.05	0.03	0.04	0.05	0.04	0.10	0.01	0.10	0.06

[a] n.d., not detected.
[b] Mg# = Mg/(Mg + Fe^{2+}) atomic ratio.
[c] Cr# = Cr/(Cr + Al) atomic ratio.
[d] Y_{Cr}, Y_{Al} and Y_{Fe} are respectively atomic ratios of Cr, Al and Fe^{3+} to $\sum$(Cr + Al + Fe^{3+}). Fe^{2+} and Fe^{3+} were calculated assuming spinel stoichiometry.

Table 2
Representative microprobe analyses (wt.%) of silicates and carbonates from the Heiani carbonate-orthopyroxenites.

Lithology	Carbonate-orthopyroxenite										
Mineral	Olivine			Orthopyroxene			Talc	Serpentine	Magnesite		
SiO_2	40.39	40.79	41.30	58.04	57.79	58.09	64.37	41.53	0.03	0.03	0.01
TiO_2	0.01	n.d.	n.d.	0.01	0.02	0.02	n.d.	n.d.	n.d.	n.d.	n.d.
Al_2O_3	n.d.	0.01	n.d.	0.07	0.07	0.06	0.12	n.d.	n.d.	n.d.	n.d.
Cr_2O_3	n.d.	n.d.	n.d.	0.05	0.12	0.00	0.12	n.d.	n.d.	n.d.	0.02
FeO	10.37	9.34	9.34	7.22	6.33	6.48	1.16	6.11	7.16	6.46	4.89
MnO	0.02	0.05	0.04	0.06	0.03	0.04	n.d.	0.04	0.10	0.13	0.10
MgO	49.28	50.11	50.90	35.05	35.58	35.54	31.04	31.77	38.99	39.12	39.04
CaO	n.d.	0.01	n.d.	0.03	0.01	0.01	n.d.	0.04	0.07	0.07	0.09
Na_2O	n.d.	0.01	n.d.	n.d.	n.d.	n.d.	0.02	n.d.	n.d.	0.01	n.d.
K_2O	n.d.	n.d.	n.d.	0.01	n.d.	n.d.	0.02	0.06	n.d.	n.d.	n.d.
NiO	0.30	0.28	0.29	0.01	0.05	0.04	0.17	0.50	0.03	0.01	0.03
Total	100.36	100.59	101.87	100.55	100.00	100.29	97.02	80.05	46.37	45.83	44.19
Cations/O =	4			6			22	7	6		
Si	0.991	0.993	0.992	1.994	1.990	1.995	8.026	2.139	0.003	0.003	0.001
Ti	0.000	0.000	0.000	0.000	0.000	0.000	0.000	0.000	0.000	0.000	0.000
Al	0.000	0.000	0.000	0.003	0.003	0.003	0.017	0.000	0.000	0.000	0.000
Cr	0.000	0.000	0.000	0.001	0.003	0.000	0.011	0.000	0.000	0.000	0.001
Fe^{2+}	0.213	0.190	0.188	0.207	0.182	0.186	0.121	0.263	0.559	0.507	0.393
Mn	0.000	0.001	0.001	0.002	0.001	0.001	0.000	0.002	0.008	0.010	0.008
Mg	1.800	1.817	1.822	1.794	1.825	1.818	5.766	2.437	5.419	5.469	5.584
Ca	0.000	0.000	0.000	0.001	0.001	0.000	0.000	0.002	0.007	0.007	0.009
Na	0.000	0.000	0.000	0.000	0.000	0.000	0.005	0.000	0.000	0.001	0.000
K	0.000	0.000	0.000	0.000	0.000	0.000	0.003	0.004	0.000	0.000	0.000
Ni	0.005	0.004	0.005	0.000	0.001	0.001	0.014	0.017	0.002	0.001	0.002
Total	3.009	3.007	3.008	4.004	4.006	4.004	13.964	4.863	5.997	5.998	5.998
Mg#	0.89	0.91	0.91	0.90	0.91	0.91	0.98	0.90	0.91	0.92	0.93

[a] Mg# = Mg/(Mg + Fe_{total}) atomic ratio.
[b] n.d., not detected.

Table 3
Representative LA-ICP-MS trace-element analyses (ppm) of metamorphic orthopyroxene from the Heiani carbonate-orthopyroxenites compared to primary orthopyroxene from the highly depleted harzburgite xenoliths of Avacha volcano, Kamchatka, Far East Russia (Ishimaru et al., 2007).

Lithology	Heiani Carb-opx			Avacha Harz.	
Opx origin	Metamorphic			Primary	
Sample No.	98A Av. (3)	96 J Av. (7)	83B Av. (3)	Av. (10)	DL
Li	1.33	1.15	0.77	1.05	0.246
B	4.96	4.15	2.59	15.13	0.348
Sc	8.35	14.87	19.28	26.45	0.077
Ti	14.56	14.27	15.84	71.53	0.461
V	8.08	9.66	11.39	96.09	0.056
Cr	381.94	372.85	227.22	4104.58	1.225
Co	81.60	85.88	88.58	54.96	0.042
Ni	245.63	264.46	355.61	644.72	1.828
Ga	1.00	1.01	0.96	nil	0.036
Rb	Nil	Nil	Nil	0.01	0.061
Sr	Nil	0.09	0.01	0.08	0.008
Y	0.62	0.78	1.09	0.06	0.002
Zr	0.01	0.01	0.01	0.04	0.003
Nb	0.01	0.01	0.02	0.03	0.004
Cs	Nil	Nil	Nil	nil	0.025
Ba	0.03	0.03	0.01	0.09	0.017
La	Nil	Nil	Nil	nil	0.003
Ce	0.01	0.01	0.01	0.01	0.002
Pr	Nil	Nil	Nil	nil	0.002
Nd	Nil	Nil	Nil	0.01	0.011
Sm	0.01	0.01	0.02	nil	0.015
Eu	Nil	Nil	Nil	nil	0.005
Gd	0.03	0.05	0.07	nil	0.010
Tb	0.01	0.02	0.02	nil	0.003
Dy	0.11	0.13	0.19	nil	0.015
Ho	0.02	0.03	0.04	nil	0.005
Er	0.05	0.06	0.08	0.01	0.009
Tm	0.01	0.01	0.01	nil	0.004
Yb	0.04	0.04	0.06	0.05	0.018
Lu	Nil	Nil	Nil	0.01	0.006
Hf	Nil	Nil	Nil	nil	0.014
Ta	Nil	Nil	Nil	nil	0.004
Pb	0.10	0.08	0.10	0.18	0.047
Th	Nil	Nil	Nil	nil	0.007
U	0.02	0.03	0.02	nil	0.006

[a] Av., average.
[b] DL, detection limits.

Trace-elements abundances of the Heiani metamorphic orthopyroxene (Fig. 9; Table 3) have been normalized to the CI chondrite values (subscript *N*) (McDonough and Sun, 1995). The chondrite-normalized pattern is generally depleted except for B, Sc and U. REEs show a slightly convex-upward depleted chondrite-normalized pattern with a flat middle- to heavy-REE level [$(Gd/Yb)_N \sim 1$] (Fig. 9). The chondrite-normalized HFSE and LILE are relatively low (Fig. 9; Table 3). Moreover, trace-element signature of the Heiani metamorphic orthopyroxene differs from that of the residual mantle orthopyroxene in harzburgite xenoliths from the Avacha volcano, Kamchatka (Ishimaru et al., 2007) (Fig. 9; Table 3). The Heiani metamorphic orthopyroxene shows characteristically convex-upward Avacha-normalized pattern in middle to heavy REEs (Fig. 9). The Ga and Y exhibit conspicuous positive anomalies, by contrast HFSE and LILE are low relative to the Avacha residual mantle orthopyroxene (Fig. 9).

The talc shows a conspicuous intragrain chemical homogeneity. It is notably highly magnesian (Mg#, ~0.97), and accordingly low in iron content (FeO^*, $\leqslant$1.2 wt.%) (Table 2). It shows relatively low NiO and Al_2O_3 respectively 0.2 and 0.1 wt.% (Table 2). The serpentine (lizardite/chrysotile) is compositionally uniform (Mg#, ~0.91). The NiO and FeO are, however, relatively high, up to 0.7 and 6 wt.%, respectively (Table 2).

Carbonates are mostly magnesites/breunnerites (Table 2). They contain 28.5–40 wt.% MgO and 2–8 wt.% FeO^*, corresponding to high and moderately restricted Mg#s (0.87–0.94) (Table 2). The CaO is generally very low (<0.1 wt.%).

6. Discussion

6.1. Petrological characteristics of the Heiani carbonate-orthopyroxenites

The area around G. Heiani (Fig. 2) has suffered a polyphase deformational history and metamorphism ranging from low-grade greenschist facies to high-grade upper-amphibolite facies (Gahlan, 2006; Gahlan and Arai, 2006). Field relations have revealed that the Heiani carbonate-orthopyroxenites (Fig. 3) cannot be considered *in situ* magmatic intrusives (e.g. Schreyer et al., 1972; Gahlan and Arai, 2009). We emphasized the Heiani carbonate-orthopyroxenites to be composed of metamorphic minerals and relict primary ones (olivine and chromian spinel). The presence of olivine, chromian spinel and (Fe, Ni) sulfides, broadly disclose a protolith of mantle origin.

Chromian spinel has been successfully used as a geotectonic indicator to distinguish between magmas from different tectonic settings (e.g. Dick and Bullen, 1984; Bonatti and Michael, 1989; Arai, 1992, 1994). The morphology of chromian spinel depends on its host peridotite lithology, it ranges from vermicular in harzburgite to euhedral in dunite, due to progressive reaction with a given melt (Matsumoto and Arai, 2001). The Cr_2O_3, Al_2O_3 and TiO_2 contents of spinel depend on their concentrations in the parental melt (Kamenetsky et al., 2001). The Cr, Al and Ti cations in chromian spinel are less or almost not affected by the post-magmatic processes (e.g. Kamenetsky et al., 2001). Hence, they are extensively used to characterize the tectonic setting. By contrast, the negative correlation between Mg# and either Cr# or FeO^* of chromian spinels (Fig. 5) may reflect variable partitioning coefficients for Mg and Fe between chromian spinel and olivine (e.g. Irvine, 1965; Dick and Bullen, 1984).

Given the above characteristics, the euhedral/rounded form of primary chromian spinels (Fig. 4A and B) combined with their high Cr#/low-TiO_2 character (Fig. 10), Al_2O_3–TiO_2 compositional relationships (Fig. 11) and absence of clinopyroxene suggest that the protolith for the Heiani carbonate-orthopyroxenites is a highly depleted peridotite (dunite or dunitic harzburgite) derived from a sub-arc setting (e.g. Dick and Bullen, 1984; Pearce et al., 1984; Bonatti and Michael, 1989; Arai, 1992, 1994; Matsumoto and Arai, 2001).

The Heiani carbonate-orthopyroxenites are characterized by the absence of anthophyllite, a characteristic of magnesian metaperidotites, because stability of the anthophyllite is reduced with increasing Mg# of peridotites (e.g. Nozaka, 2011). The latter observation is in line with absence of the magnetite overgrowths around chromian spinel. As far as well known, alterations of spinel and magnetite formation are related to the surrounding silicate matrix (e.g. Barnes, 2000). The Heiani silicate matrix is magnesian; hence the expected amount of released iron upon olivine hydration is small.

The highly depleted peridotite protolith from the Heiani ophiolite may have had a genetic link with boninites/high-Mg arc tholeiites. Highly depleted peridotites with high Cr# ($\geqslant$0.7) of spinel are very common in the Precambrian ophiolites (e.g. Quick, 1990; Liipo et al., 1995; Gahlan, 2006 and references therein), and not uncommon in Phanerozoic ones (e.g. England and Davies, 1973; Ishiwatari et al., 2003 and references therein).

The olivine, which occurs as relics in orthopyroxene (Fig. 4A and B), is primary and falls in the chemical range of mantle olivine (Fig. 6; Table 2) (e.g. Vance and Dungan, 1977; Takahashi, 1987; Rudnick et al., 1993). The relict olivine in the Heiani

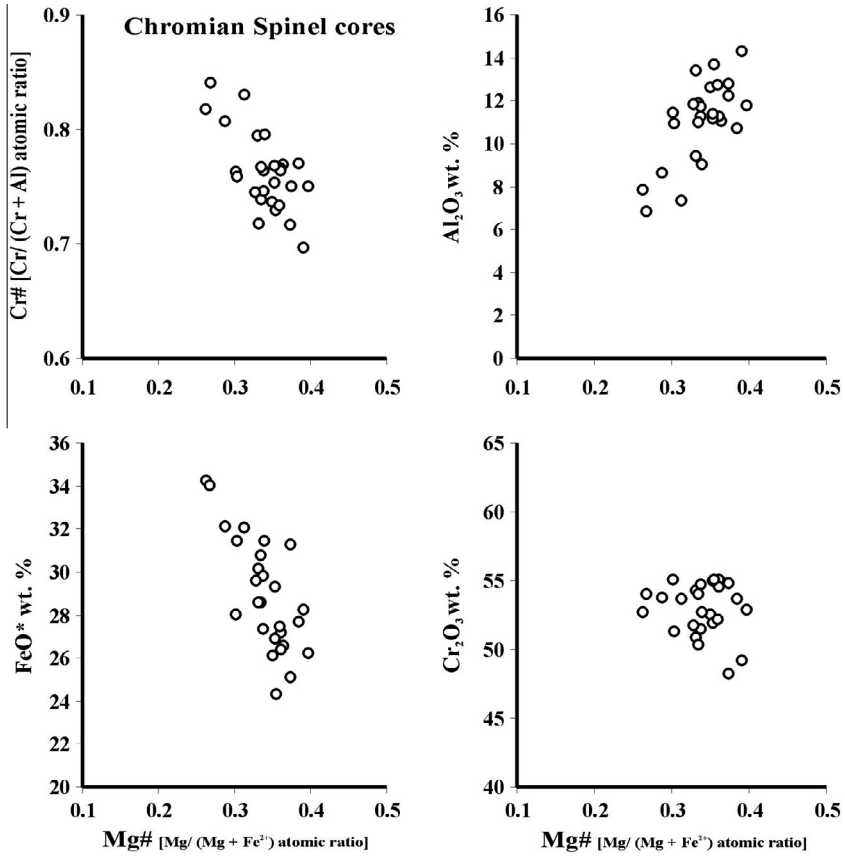

Fig. 5. Relations between Mg# and Cr#, Al_2O_3, FeO^* and Cr_2O_3 (wt.%) of primary chromian spinel cores from the Heiani carbonate-orthopyroxenites.

carbonate-orthopyroxenites is commonly clear and free from opaque minute inclusions, its Mg# and NiO contents are respectively (0.88–0.92) and (0.25–0.4) (e.g. Arai, 1975; Gahlan and Arai, 2009). By contrast, the metamorphic olivine would form megacrysts, and would contain either opaque minute inclusions or relicts of antigorite, talc and/or magnesite (e.g. Gahlan, 2006). Where, it can be developed at the expenses of antigorite, or talc and magnesite by either increasing the mole fraction of H_2O or temperature (e.g. Johannes, 1969).

Petrographic characteristics of the Heiani orthopyroxene (Fig. 4) combined with low contents of Ca, Cr and Al (Fig. 7) indicate a metamorphic origin (e.g. Evans and Trommsdorff, 1974; Arai, 1975; Pinsent and Hirst, 1977; Trommsdorff et al., 1998; Katzir et al., 1999; Gahlan and Arai, 2009). Moreover, in Fig. 12 the Heiani orthopyroxene falls clearly in the field of regional metamorphic orthopyroxenes. The Ca, Cr and Al contents in orthopyroxene are function of temperature (e.g. Arai, 1975; Danckwerth and Newton, 1978; Gasparik and Newton, 1984; Grove et al., 2006). Accordingly, low Ca, Cr and Al contents in the Heiani metamorphic orthopyroxene (Figs. 7 and 12) can be attributed to low temperature of crystallization and possible depletion of these elements in the peridotite (serpentinite) precursor. Furthermore, the intragrain chemical homogeneity (i.e. absence of zonation) confirms the orthopyroxene's low temperature of crystallization.

The Mg–Fe distribution coefficients (K_D) between olivine and orthopyroxene are known to be insensitive to equilibration temperature (Matsui and Nishizawa, 1974). In our rocks, the metamorphic orthopyroxene shows a wider range of Mg# than the associated primary olivine (Fig. 8). Compared to the Alpine-type Ol–Opx pairs ($K_D \approx 1$; Trommsdorff and Evans, 1974), K_D between the Heiani Ol–Opx pairs clearly deviates from unity ($K_D = 0.8–1.2$; Fig. 8), indicating chemical disequilibrium.

Up to now, the trace elements characteristics of metamorphic orthopyroxenes have not been well established in the literatures. The trace element signature (Fig. 9; Table 3) of the Heiani metamorphic orthopyroxene was probably controlled by a combination of factors; mainly trace element characteristics of the peridotite (serpentinite) protolith and composition of the impure carbonates in the adjacent metasediments.

Concentrations of the incompatible trace elements in bulk-rock peridotites decrease concurrently with increasing degree of the partial melting. Moreover, the contribution of chromian spinels to the incompatible trace elements budget of bulk-rock peridotites is negligible (Bedini and Bodinier, 1999). Consequently, we expect a low trace element budget for the peridotite protolith of the Heiani carbonate-orthopyroxenites.

The markedly positive Ga, Y and U anomalies (Fig. 9; Table 3) are inferred to reflect the trace element signature of the metasomatising agent/fluids. U, Y and REEs are sensitive to depth and setting of the shelf carbonate successions (e.g. Guo et al., 2013 and reference therein). The low trace-elements contents of the Heiani orthopyroxene (Fig. 9A; Table 3) likely confirm the metamorphic/metasomatic origin (e.g. Adam et al., 1997). The Characteristic convex-upward Avacha-normalized pattern in middle to heavy REEs of the Heiani orthopyroxene (Fig. 9B; Table 3) is probably due to lower incompatibility and lower mobility of these elements during alteration and/or metasomatism (e.g. Hellebrand et al., 2001).

6.2. Tectono-metamorphic evolution of the Heiani carbonate-orthopyroxenites

6.2.1. Deformation phases versus metamorphic events

Apart of the dynamic deformation and diaphthoresis along shear zones, the Tiers I and II respectively the gneisses and

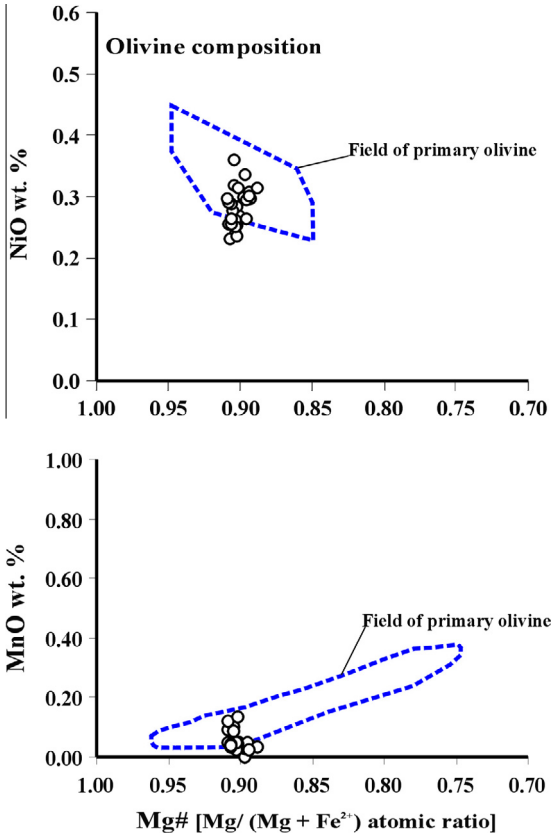

Fig. 6. NiO and MnO (wt.%) versus Mg# of olivine in carbonate-orthopyroxenites from the Heiani ophiolite. The fields of mantle olivine for NiO and MnO are from Takahashi (1987) and Rudnick et al. (1993), and Vance and Dungan (1977), respectively.

structurally overlying nappes have suffered a polyphase deformational history (D_{1-3}) and four metamorphic events (M_{0-3}).

M_0 is equal to the ocean-floor metamorphism that has affected ophiolites prior to thrusting. M_1 is the low-grade regional metamorphism that accompanied the ophiolite obduction. Being syn-kinematic with M_1, the D_1 phase of deformation is expressed by thrusting and folding, represented by the NW–SE-trending/S-verging folds (Fig. 2). The D_1 phase of deformation, acting over a long time-span, is pertaining to an early N–S collision stage between the Gabgaba terrane and the SED terrane (Fig. 1) (e.g. Zoheir and Klemm, 2007; Abdeen and Abdelghaffar, 2011). M_2 is the low-*P*/high-*T* regional metamorphism that has been caused by ascent of the syn-orogenic large granitic batholiths at depth (e.g. Droop and Al-Filali, 1989). The latter metamorphic event leads to development of (muscovite, biotite, almandine, staurolite, kyanite and cordierite-bearing) schists and gneisses, up to migmatites in the Tire I rocks (ca. 660 Ma; Stern et al., 1989). Being synchronous with M_2, the D_2 phase of deformation developed large-scale NNW–SSE-trending folds and major dextral strike slip faults (e.g. HSZ) (Fig. 2). The D_2 phase of deformation corresponds to a late collisional stage during the Pan-Africa terrane accretion and the E–W crustal shortening (ca. 650–620 Ma) (e.g. Kröner and Stern, 2004; Zoheir and Klemm, 2007). M_3 is the local contact metamorphism superimposed on the regional metamorphism (M_1 and M_2), particularly around syn- to late-orogenic granodiorite to monzogranite intrusions (Fig. 2). Being synchronous with M_3, the D_3 phase of deformation continued the dextral shearing movements, and tightened, stretched and clock-wise rotated the NNW–SSE-trending folds to acquire an N–S trend. The D_3 phase of deformation pertains to crustal shortening and escape tectonics (ca. 630–550 Ma) (e.g. Zoheir and Klemm, 2007).

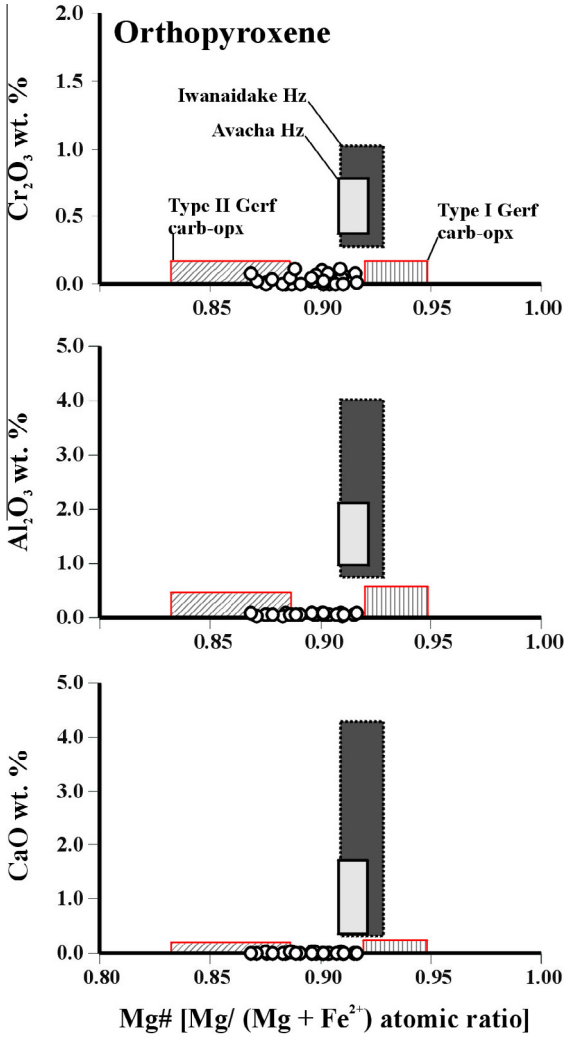

Fig. 7. Relations between Mg# and Cr_2O_3, Al_2O_3 and CaO (wt.%) of metamorphic orthopyroxene from the Heiani carbonate-orthopyroxenites. Data for the Gerf carbonate-orthopyroxenites (Gahlan and Arai, 2009), and the Iwanaidake (Kubo, 2002) and Avacha (Ishimaru et al., 2007) harzburgites are given for comparison.

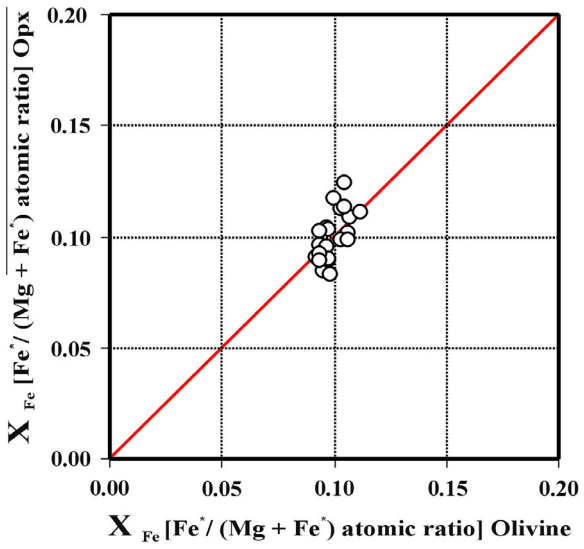

Fig. 8. Distribution of iron and magnesium between coexisting olivines and orthopyroxenes (Opx) from the Heiani carbonate-orthopyroxenites.

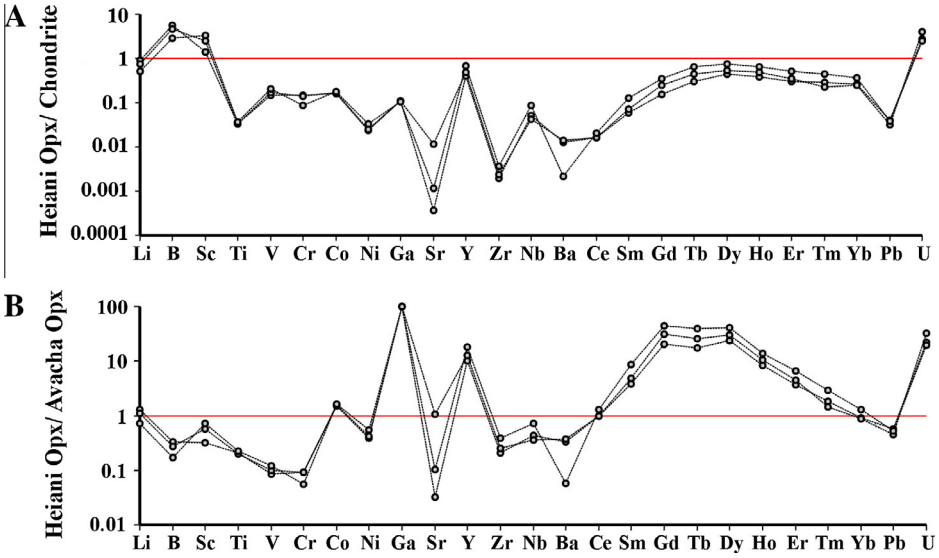

Fig. 9. Trace-element pattern of metamorphic orthopyroxene (Opx) from the Gerf carbonate-orthopyroxenites. (A) Normalized to chondrite values (McDonough and Sun, 1995). (B) Normalized to primary orthopyroxene values from the highly depleted harzburgite mantle xenoliths of Avacha volcano, Kamchatka, Russia (Ishimaru et al., 2007).

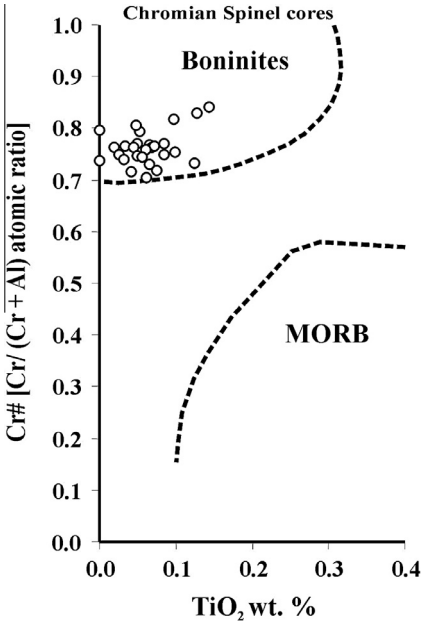

Fig. 10. Relations between TiO_2 (wt.%) and Cr# of primary chromian spinel cores in carbonate-orthopyroxenites from the Heiani ophiolite. The fields of boninites and MORB are from Arai (1992).

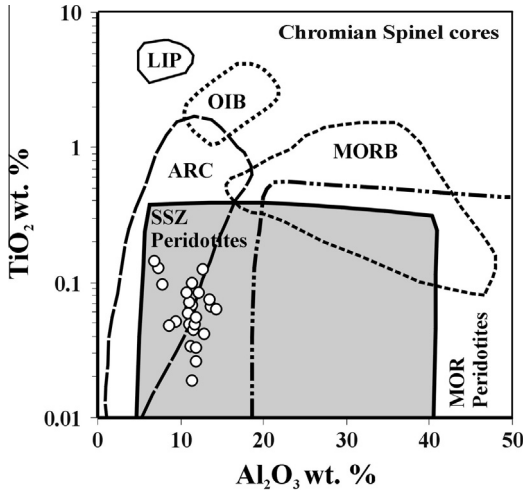

Fig. 11. Relations between Al_2O_3 and TiO_2 (wt.%) of primary chromian spinel cores in carbonate-orthopyroxenites from the Heiani ophiolite. The fields of SSZ and MORB peridotites, and LIP, OIB, ARC and MORB are given for comparison after Kamenetsky et al. (2001).

6.2.2. Metamorphic conditions

Johannes (1970) gives an estimate on stability of the enstatite + magnesite (E + M) paragenesis at pressures up to 10 kbar (Fig. 13). Following Johannes's (1970) estimate, we can conclude that the required CO_2 content for the formation of the (E + M) paragenesis will decrease from $X_{CO2} = 0.6$ at 7 kbar to 0.35 at 10 kbar (Fig. 13). Fig. 14 gives an estimate for the stability range of the assemblage (E + M) (e.g. Johannes, 1969, 1970; Schreyer et al., 1972). It is noteworthy that the experimental system of Johannes (1969, 1970) is an ideal one (Fe-free), which is slightly different from the actual rocks. The assemblage (E + M) breaks down to form forsterite at higher *T* and/or lower *P*, and (quartz + magnesite) at lower *T* and/or higher *P* (Fig. 14). The latter phase relations prove that carbonate-orthopyroxenites cannot exist at magmatic conditions (e.g. Johannes, 1969; Schreyer et al., 1972; Gahlan and Arai, 2009).

A comparison with *P*/*T* stability data of index minerals in the adjacent country rocks will help confirm and disclose the metamorphic/metasomatic conditions of the studied carbonate-orthopyroxenites. Typical country rocks of the Heiani carbonate-orthopyroxenites are: kyanite–muscovite schists, kyanite-bearing biotite gneisses, migmatites, granite gneisses and mobilizates (cordierite aploids and kyanite–quartz veins) (Gahlan, 2006). The lower pressure stability limit of kyanite (e.g. Richardson et al., 1969) intersects the (E + M) band at *P*/*T* near the Al_2SiO_5 triple point (Fig. 14). The migmatites or granite gneisses put the *P*/*T* conditions of the latter high-grade country rocks above the minimum melting of granite (e.g. Luth et al., 1964) (Fig. 14). In addition, the presence of cordierite in the country rocks restricts the *P*/*T* range in the shaded field within the (E + M) band (Fig. 14). Accordingly, the expected *P*/*T* metamorphic conditions are: 630–645 °C and 6–6.5 kbar (Fig. 14).

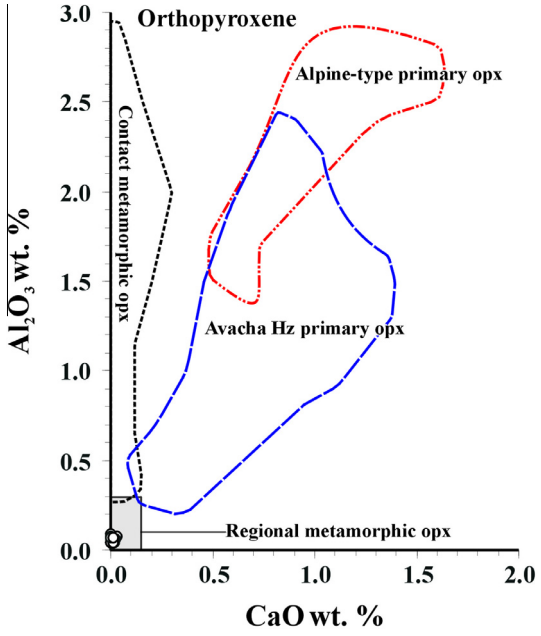

Fig. 12. Relations between CaO and Al_2O_3 (wt.%) of metamorphic orthopyroxene from the Heiani carbonate-orthopyroxenites. The fields of orthopyroxenes from the Alpine-type peridotites (Arai, 1980; Pinsent and Hirst, 1977), Avacha highly depleted harzburgite mantle xenoliths (Ishimaru et al., 2007), regionally metamorphosed ultramafics (Evans and Trommsdorff, 1974; Trommsdorff et al., 1998) and contact metamorphosed ultramafics (Arai, 1975; Frost, 1975) are all given for comparison.

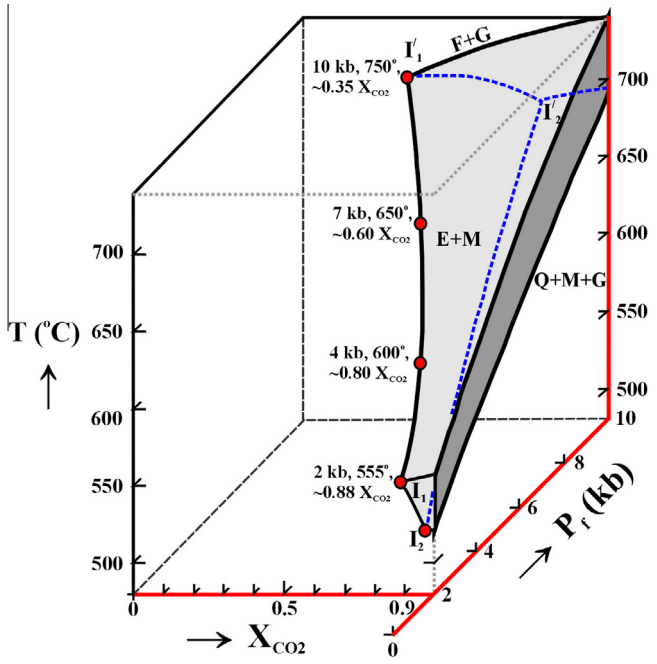

Fig. 13. Isobaric equilibrium conditions of reactions occurring at large X_{CO2} and relatively elevated P/T values for the assemblage (Enstatite + Magnesite) (Johannes, 1970). F, olivine (forsterite); E, orthopyroxene (enstatite); M, magnesite; Q, quartz; G, CO_2. The solid dots represent P–T–X_{CO2} locations of the isobaric invariant points.

It seems that the Heiani serpentinized peridotites have reacted with CO_2-rich/H_2O-poor fluid phase to develop carbonate-orthopyroxenites in close juxtaposition and simultaneously with their country rocks under essentially identical P/T conditions (e.g. Johannes, 1969; Schreyer et al., 1972). Furthermore, the presence

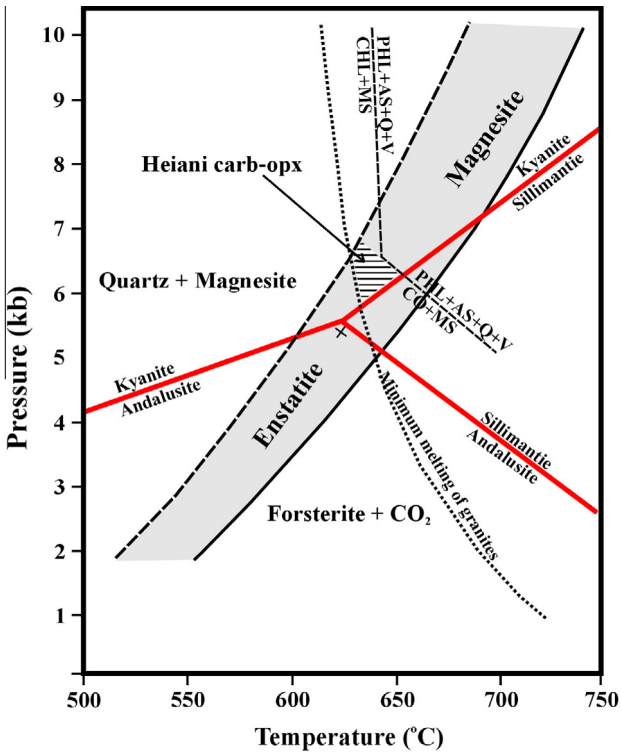

Fig. 14. P/T conditions for the stable assemblage (E + M) within a band under high-enough X_{CO2}. Stability fields of the Al_2SiO_5 polymorphs, the (phlogopite + Al_2SiO_5 + quartz) assemblage, and the minimum melting curve of granites are given for geothermo-barometric comparison (e.g. Johannes, 1969, 1970; Schreyer et al., 1972). The shaded field within the (E + M) band suggests P/T metamorphic conditions of the Heiani carbonate-orthopyroxenites based on a comparison with P/T stability data of the index minerals in the adjacent country rocks. It represents the intersection between: the lower pressure stability limit of kyanite, migmatites P/T conditions above the minimum melting of granite curve and the upper P/T stability limit of cordierite; all within the (E + M) band. AS, Al_2SiO_5; CHL, chlorite; PHL, phlogopite; MS, muscovite; CO, cordierite; V, vapor; Q, quartz.

of quartz feldspathic gneisses, granodiorite diatexites and kyanite–quartz veins indicate a water-deficient partial melting. The water deficiency is a prerequisite condition to form carbonate-orthopyroxenites, i.e. high X_{CO2}.

The massive fabric of the Heiani carbonate-orthopyroxenites (Fig. 3) is due to metasomatism, up to the upper-amphibolite facies, on possibly rigid unsheared precursor. By similarity, regional metamorphism (at least 630 °C, 6 kbar and high-X_{CO2}) of a peridotite precursor resulted in formation of the carbonate-orthopyroxenites of the type locality, Troms, Norway (Schreyer et al., 1972). Whereas, thermal metamorphism (520–560 °C, 2 kbar and 0.87–1 X_{CO2}) resulted in the formation of the Gerf carbonate-orthopyroxenites, SED, Egypt (Gahlan and Arai, 2009).

We believe that only CO_2, as a metasomatising agent, had been introduced, because the resulting rocks contain the newly formed orthopyroxene and magnesite in approximately equal molar ratios (e.g. Johannes, 1969; Gahlan and Arai, 2009). The ratio of orthopyroxene/magnesite is the most important difference between the Heiani carbonate-orthopyroxenites and those of the type locality, Troms, Norway (e.g. Schreyer et al., 1972).

6.3. Source and mechanism of the metasomatising agent (CO_2-rich fluids)

A variety of sources have been proposed for origin of CO_2-rich fluids: (1) groundwater descending from the zone of weathering (e.g. Kralik et al., 1989; Jedrysek and Halas, 1990), (2) ascending

diagenetic–metamorphic fluids (e.g. Vakanjak et al., 1984), (3) volcanism-related fluids, (4) granite-related fluids (e.g. Raymond, 2002) and (5) mantle degassing products (e.g. Veizer et al., 1989).

Origin of the northeastern African basement carbonates is a matter of debate. Based on C, O and Sr isotopic compositions, Stern and Gwinn (1990) and Pitcairn et al. (2013) concluded that origin of the Neoproterozoic basement carbonates from the Central Eastern Desert of Egypt and northern Sudan is best explained by mixing between remobilized sedimentary carbonates and mantle fluids. A spatial relation and positive correlation between existence of marble/carbonate-bearing metasedimentary layers, shear zones and carbonatization of the Heiani serpentinites has been observed. Hence, we propose that source of the Heiani metasomatising CO_2-rich fluids was the neighboring impure carbonate layers of shelf sedimentary origin (e.g. Kelemen et al., 2011; Beinlich et al., 2012). Although, a mixed sedimentary-mantle C source is not unlikely (an isotope study will be a subject for future research). It is well known that siliceous carbonates release CO_2 during progressive metamorphism (e.g. Schreyer et al., 1972; Evans and Trommsdorff, 1974; Baker and Matthews, 1994; Raymond, 2002). Moreover, there is a positive correlation between the released amount of CO_2 and the degree of metamorphism (e.g. Raymond, 2002).

Infiltration of the ultramafic terranes by CO_2-bearing hydrothermal fluids results in a wide spectrum of (possibly mineralized) carbonated meta-ultramafics (e.g. Halls and Zhao, 1995; Akbulut et al., 2006 and references therein). Formation of the carbonated meta-ultramafics is structurally controlled; where faults act as conduits for the hydrothermal fluids input (e.g. Auclair et al., 1993; Uçurum, 2000; Akbulut et al., 2006). Hence, we propose that at a late collisional stage during the Pan-Africa terrane accretion and the E–W crustal shortening (D_2 and D_3) (ca. 650–620 Ma; Kröner and Stern, 2004; Zoheir and Klemm, 2007), low-*P*/high-*T* regional metamorphism (M_2) (ca. 660 Ma; Stern et al., 1989) took place and metamorphism attained its peak conditions. The latter metamorphism, which affected the carbonate-bearing shelf sediments beneath and/or in juxtaposition with the Heiani ophiolite, induced decarbonation reactions and pervasive release of CO_2. On the other hand, N–S-shearing enhanced permeability of the host rocks and facilitate invasion of the hydrothermal fluids. The N–S deep seated faults and shear zones have tapped CO_2 that caused the metasomatism seen in the Heiani carbonate-orthopyroxenite rocks. The latter mechanism explains the close relation between carbonatized metaperidotites and shear zones. Accordingly, the Heiani carbonate-orthopyroxenites can be regarded as shear-related reaction zones.

6.4. Applications and environmental impact

A part of their importance in mineral exploration (particularly gold), the carbonated meta-ultramafics represent a natural analogue to CO_2 sequestration via *in situ* mineral carbonation (e.g. Seifritz, 1990). CO_2 is chemically bound in the form of carbonate minerals by reaction with Mg^{2+} and/or Ca^{2+} that deliberated from silicates. The carbonation reactions are controlled mainly by: the pre-existing fault/fracture permeability systems, the activity of CO_2 in the fluid phase, temperature, the time available for carbonation and the flow velocities (e.g. Hansen et al., 2005).

7. Conclusions

(1) Highly depleted serpentinized dunites or dunitic harzburgites derived from a sub-arc setting are the inferred protolith of the Heiani carbonate-orthopyroxenites (based on spinel opposition and morphology).
(2) Low-*P*/high-*T* regional metamorphism (M_2), up to the upper-amphibolite facies, accompanied by CO_2-metasomatism, affected the Heiani serpentinized peridotites and resulted in formation of the carbonate-orthopyroxenites along shear zones that acted as fluid conduits.
(3) The prevailing metamorphic conditions during formation of the Heiani carbonate-orthopyroxenites are: 630–650 °C, 6–7 kbar (20–23 km depth) and high-X_{CO2} (0.6–0.7).
(4) Among a complicated combination of factors, lithology and tectonics control formation of the Heiani carbonate-orthopyroxenites.
(5) The elongate prismatic habit, absence of chemical zonation or exsolution lamellae of Ca-rich pyroxene, extreme depletion in Ca, Al and Cr, and MREE enrichment are textural and chemical characteristics of the metamorphic orthopyroxenes.
(6) The carbonate-bearing shelf sediments beneath and/or in juxtaposition with the Heiani ophiolite are the likely source of the metasomatising CO_2-rich fluids.
(7) A late collisional stage during the Pan-Africa terrane accretion and the E–W crustal shortening (ca. 650–620 Ma) is the suggested episode/relative age of the Heiani carbonate-orthopyroxenites' formation; i.e. postdates the ophiolite obduction.
(8) The ultramafic terranes are of environmental impact, where they can be enhanced to develop a sink for atmospheric CO_2.

Acknowledgments

H.A.G. and S.A.A. owe the debt of gratitude to King Saud University, Deanship of Scientific Research, College of Science, Research Center, for supporting the current research. The sincere appreciation has been expressed to T. Morishita for his support in the microprobe and LA-ICP-MS analyses. H.A.G. is indebted to A. Kröner for useful discussions about the Arabian Nubian Shield terranes. Also, the sincere thanks are extended to A. Khudeir for his assistance in mapping the region around G. Heiani area. We are grateful to two anonymous reviewers for their highly constructive comments that improved the manuscript. Special thanks are paid to Read Mapeo for his editorial handling.

References

Abdeen, M.M., Abdelghaffar, A.A., 2011. Syn- and post-accretionary structures in the Neoproterozoic Central Allaqi-Heiani suture zone, Southeastern Egypt. Precambr. Res. 185, 95–108.
Abdelsalam, M.G., Stern, R.J., 1996. Sutures and shear zones in the Arabian-Nubian Shield. J. Afr. Earth Sc. 23, 289–310.
Abdelsalam, M.G., Abdeen, M.M., Dowaidar, H.M., Stern, R.J., Abdelghaffar, A.A., 2003. Structural evolution of the Neoproterozoic Western Allaqi-Heiani suture, southeastern Egypt. Precambr. Res. 124, 87–104.
Adam, J., Green, T.H., Sie, S.H., Ryan, C.G., 1997. Trace element partitioning between aqueous fluids, silicate melts and minerals. Eur. J. Mineral. 9, 569–584.
Akbulut, M., Pişkin, Ö., Karayiğit, A.I., 2006. The genesis of the carbonatized and silicified ultramafics known as listvenites: a case study from the Mihalıççık region (Eskişehir), NW Turkey. Geol. J. 41, 557–580.
Ali, K.A., Azer, M.K., Gahlan, H.A., Wilde, S.A., Samuel, M.D., Stern, R.J., 2010. Age constraints on the formation and emplacement of Neoproterozoic ophiolites along the Allaqi-Heiani Suture, South Eastern Desert of Egypt. Gondwana Res. 18, 583–595.
Anonymous, 1972. Penrose field conference on ophiolites. Geotimes 17, 24–25.
Arai, S., 1975. Contact metamorphosed dunite–harzburgite complex in the Chugoku district, western Japan. Contrib. Miner. Petrol. 52, 1–16.
Arai, S., 1980. Dunite–harzburgite–chromitite complexes as refractory residue in the Sangun-Yamaguchi zone, western Japan. J. Petrol. 21, 141–165.
Arai, S., 1992. Chemistry of chromian spinel in volcanic rocks as a potential guide to magma chemistry. Mineral. Mag. 56, 173–184.
Arai, S., 1994. Compositional variation of olivine–chromian spinel in Mg-rich magmas as a guide to their residual spinel peridotites. J. Volcanol. Geoth. Res. 59, 279–293.
Auclair, M., Gauthier, M., Trottier, J., Jébrak, M., Chartrand, F., 1993. Mineralogy,

geochemistry, and paragenesis of the Eastern Metals serpentinite-associated Ni–Cu–Zn deposit, Quebec Appalachians. Econ. Geol. 88, 123–138.
Baker, J., Matthews, A., 1994. Textural and isotopic development of marble assemblages during the Barrovian-style M_2 metamorphic event, Naxos, Greece. Contrib. Miner. Petrol. 116, 130–144.
Barnes, S.J., 2000. Chromite in komatiites, II. Modification during greenschist to mid-amphibolite facies metamorphism. J. Petrol. 41, 387–409.
Barth, T.F.W., 1926. Sagvandite, a magnesite bearing igneous rock. Norsk Geol. Tidsskr. 9, 271–303.
Bedini, R.M., Bodinier, J.-L., 1999. Distribution of incompatible trace elements between the constituents of spinel peridotite xenoliths: ICP-MS data from the East African Rift. Geochim. Cosmochim. Acta 63, 3883–3900.
Beinlich, A., Plümper, O., Hövelmann, J., Austrheim, H., Jamtveit, B., 2012. Massive serpentinite carbonation at Linnajavri, N-Norway. Terra Nova 24, 446–455.
Bonatti, E., Michael, P.J., 1989. Mantle peridotites from continental rifts to ocean basins to subduction zones. Earth Planet. Sci. Lett. 91, 297–311.
Danckwerth, P.A., Newton, R.C., 1978. Experimental determination of the spinel peridotite to garnet peridotite reaction in the system $MgO–Al_2O_3–SiO_2$ in range 900–1100 °C and Al_2O_3 isopleths of enstatite in the spinel field. Contrib. Miner. Petrol. 66, 189–201.
de Wall, H., Greiling, R.O., Sadek, M.F., 2001. Post-collisional shortening in the late Pan-African Hamisana high Strain Zone, SE Egypt: filed and magnetic fabric evidence. Precambr. Res. 107, 179–194.
Dick, H.J.B., Bullen, T., 1984. Chromian spinel as a petrogenetic indicator in abyssal and Alpine-type peridotites and spatially associated lavas. Contrib. Miner. Petrol. 86, 54–76.
Droop, G.T.R., Al-Filali, I.Y., 1989. Magmatism, deformation and high-T, low-P regional metamorphism in the Nabitah mobile belt, southern Arabian Shield. In: Daly, J.S., Cliff, R.A., Yardley, B.W.D. (Eds.), Evolution of Metamorphic Belts. Geological Society, London, Special Publications 43, pp. 469–480.
El Gaby, S., List, N.K., Tehrani, R., 1988. Geology, evolution and metallogenesis of the Pan-African Belt in Egypt. In: El Gaby, S., Greiling, R.O. (Eds.), The Pan-African Belt of Northeast Africa and Adjacent Areas. Vieweg & Sohn, Braunschweig/Wiesbaden, pp. 17–68.
England, R.N., Davies, H.L., 1973. Mineralogy of ultramafic cumulates and tectonites from eastern Papua. Earth Planet. Sci. Lett. 17, 416–425.
Evans, B.W., Trommsdorff, V., 1974. Stability of enstatites + talc, and CO_2-metasomatism of metaperidotite, Val d'efra, Lepontine Alps. Am. J. Sci. 274, 274–296.
Frost, B.R., 1975. Contact metamorphism of serpentinite, chloritic blackwall and rodingite at Paddy-Go-Easy Pass, central Cascades, Washington. J. Petrol. 16, 272–313.
Gahlan, H.A., 2006. Petrological Characteristics of the Mantle Section in the Proterozoic Ophiolites from the Pan-African Belt. Ph.D. Thesis. Kanazawa University.
Gahlan, H.A., Arai, S., 2006. Petrological Characteristics and CO_2-Metasomatism of Wadi Fiqo Mantle Peridotites of the Pan-African Proterozoic Ophiolite, South Eastern Desert, Egypt. Oral Presentation and Abstract at The Sixth International Conference on the Geology of The Middle East, Al-Ain, UAE, 20–22, March 2006, A-171.
Gahlan, H.A., Arai, S., 2009. Carbonate-orthopyroxenite lenses from the Neoproterozoic Gerf ophiolite, South Eastern Desert, Egypt: the first record in the Arabian Nubian Shield ophiolites. J. Afr. Earth Sc. 53, 70–82.
Gasparik, T., Newton, R.C., 1984. The reversed alumina content of orthopyroxene in the equilibrium with spinel and forsterite in the system $MgO–Al_2O_3–SiO_2$. Contrib. Miner. Petrol. 85, 186–196.
Greiling, R.O., Abdeen, M.M., Dardir, A.A., El Akhal, H., El Ramly, M.F., Kamal El Din, G.M., Osman, A.F., Raswan, A.A., Rice, A.H.N., Sadek, M.F., 1994. A structural synthesis of the Proterozoic Arabian-Nubian Shield in Egypt. Geol. Rundsch. 83, 484–501.
Grove, T.L., Chatterjee, N., Parman, S.W., Médard, E., 2006. The influence of H_2O on mantle wedge melting. Earth Planet. Sci. Lett. 249, 74–89.
Guo, H., Du, Y., Zhou, L., Yang, J., Huang, H., 2013. Trace and rare earth elemental geochemistry of carbonate succession in the Middle Gaoyuzhuang Formation, Pingquan Section: implications for Early Mesoproterozoic ocean redox conditions. J. Palaeogeogr. 2, 209–221.
Halls, C., Zhao, R., 1995. Listvenite and related rocks: perspectives on terminology and mineralogy with reference to an occurrence at Cregganbaun, Co. Mayo, Republic of Ireland. Miner. Deposita 30, 303–313.
Hansen, L.D., Dipple, G.M., Gordon, T.M., Kellett, D.A., 2005. Carbonated serpentinite (listwanite) at Atlin, British Columbia: a geological analogue to carbon dioxide sequestration. Can. Mineral. 43, 225–239.
Hellebrand, E., Snow, J.E., Dick, H.J.B., Hofmann, A.W., 2001. Coupled major and trace elements as indicators of the extent of melting in mid-ocean-ridge peridotites. Nature 410, 677–681.
Irvine, T.N., 1965. Chromian spinel as a petrogenetic indicator: Part 1. Theory. Can. J. Earth Sci. 2, 648–671.
Ishida, Y., Morishita, T., Arai, S., Shirasaka, M., 2004. Simultaneous *in-situ* multi-element analysis of minerals on thin section using LA-ICP-MS. Sci. Rep. Kanazawa Univ. 48, 31–42.
Ishimaru, S., Arai, S., Ishida, Y., Shirasaka, M., Okrugin, V.M., 2007. Melting and multi-stage metasomatism in the mantle wedge beneath a frontal arc inferred from highly depleted peridotite xenoliths from the Avacha Volcano, Southern Kamchatka. J. Petrol. 48, 395–433.
Ishiwatari, A., Sokolov, S.D., Vysotskiy, S.V., 2003. Petrological diversity and origin of ophiolites in Japan and Far East Russia with emphasis on depleted harzburgite. In: Dilek, Y., Robinson, P.T. (Eds.), Ophiolites in Earth History. Geological Society, London, Special Publications 218, pp. 597–617.
Jedrysek, M.O., Halas, S., 1990. The origin of magnesite deposits from the Polish Foresudetic block ophiolites: preliminary $\delta^{13}C$ and $\delta^{18}O$ investigations. Terra Nova 2, 154–159.
Johannes, W., 1969. An experimental investigation of the system $MgO–SiO_2–H_2O–CO_2$. Am. J. Sci. 267, 1083–1104.
Johannes, W., 1970. Zur Entstehung von Magnesitvorkommen. Neues Jahrb. Mineral., Abh. 113, 274–325.
Kamenetsky, V.S., Crawford, A.J., Meffre, S., 2001. Factors controlling chemistry of magmatic spinel: an empirical study of associated olivine, Cr-spinel and melt inclusions from primitive rocks. J. Petrol. 42, 655–671.
Katzir, Y., Avigad, D., Matthews, A., Garfunkel, Z., Evans, B.W., 1999. Origin and metamorphism of ultrabasic rocks associated with a subducted continental margin, Naxos (Cyclades, Greece). J. Metamorph. Geol. 17, 301–318.
Kelemen, P.B., Matter, J., Streit, E.E., Rudge, J.F., Curry, W.B., Blusztajn, J., 2011. Rates and mechanisms of mineral carbonation in peridotite: natural processes and recipes for enhanced, in situ CO_2 capture and storage. Annu. Rev. Earth Planet. Sci. 39, 545–576.
Kralik, M., Aharon, P., Schroll, E., Zachmann, D., 1989. Carbon and oxygen isotope systematics of magnesites: a review. In: Moller, P. (Ed.), Magnesite: Geology, Mineralogy, Geochemistry and Formation of Mg Carbonates. Monograph Series on Mineral Deposits 28, Borntraeger, Berlin, pp. 197–223.
Kröner, A., Stern, R.J., 2004. Africa/Pan-African orogeny. Encycl. Geol. 1, 1–12.
Kröner, A., Greiling, R., Reischmann, T., Hussein, I.R.M., Stern, R.J., Dürr, S., Krüger, J., Zimmer, M., 1987. Pan-African crustal evolution in the Nubian segment of Northeast Africa. In: Kröner, A. (Ed.), Proterozoic Lithosphere Evolution. American Geophysical Union Geodynamics Series 17, pp. 235–257.
Kröner, A., Todt, W., Hussein, I.M., Mansour, M., Rashwan, A., 1992. Dating of Late Proterozoic ophiolites in Egypt and Sudan using the single grain zircon evaporation technique. Precambr. Res. 59, 15–32.
Kubo, K., 2002. Dunite formation processes in highly depleted peridotite: case study of Iwanaidake peridotite, Hokkaido, Japan. J. Petrol. 43, 423–448.
Liipo, J., Vuollo, J., Nykänen, V., Piirainen, T., Pekkarinen, L., Tuokko, I., 1995. Chromites from the early Proterozoic Outokumpu-Jormua ophiolite belt: a comparison with chromites from Mesozoic ophiolites. Lithos 36, 15–27.
Loney, R.L., Himmelberg, G.R., Coleman, R.G., 1971. Structure and petrology of the alpine-type peridotite at Burro Mountain, California, USA. J. Petrol. 12, 245–309.
Longerich, H.P., Jackson, S.E., Günther, D., 1996. Laser ablation inductively coupled plasma mass spectrometry transient signal data acquisition and analyte concentration calculation. J. Anal. At. Spectrom. 11, 899–904.
Luth, W.C., Jahns, R.H., Tuttle, O.F., 1964. The granite system at pressures of 4 to 10 kilobars. J. Geophys. Res. 69, 759–773.
Matsui, Y., Nishizawa, O., 1974. Iron (II)-magnesium exchange equilibrium between olivine and calcium-free pyroxene over a temperature range 800 °C to 1300 °C. Bull. Soc. Française Minéral. Cristallogr. 97, 122–130.
Matsumoto, I., Arai, S., 2001. Morphological and chemical variations of chromian spinel in dunite–harzburgite complexes from the Sangun zone (SW Japan): implications for mantle/melt reaction and chromitite formation processes. Mineral. Petrol. 73, 305–323.
McDonough, W.F., Sun, S.-S., 1995. The composition of the earth. Chem. Geol. 120, 223–253.
Morishita, T., Ishida, Y., Arai, S., Shirasaka, M., 2005. Determination of multiple trace element compositions in thin (<30 μm) laser of NIST SRM 614 and 616 using laser ablation-inductively coupled plasma-mass spectrometry (LA-ICP-MS). Geostand. Geoanal. Res. 29, 107–122.
Moussa, E.M., Stern, R.J., Manton, W.I., Ali, K., 2008. SHRIMP zircon dating and Sm/Nd isotopic investigations of Neoproterozoic granitoids, Eastern Desert, Egypt. Precambr. Res. 160, 341–356.
Nozaka, T., 2011. Constraints on anthophyllite formation in thermally metamorphosed peridotites from southwestern Japan. J. Metamorph. Geol. 29, 385–398.
Pearce, J.A., Lippard, S.J., Roberts, S., 1984. Characteristics and tectonic significance of supra-subduction zone ophiolites. In: Kokelaar, B.P., Howells, M.F. (Eds.), Marginal Basin Geology. Geological Society, London, Special Publication 16, pp. 77–94.
Pearce, N.J.G., Perkins, W.T., Westgate, J.A., Gorton, M.P., Jackson, S.E., Neal, C.R., Chenery, S.P., 1997. A compilation of new and published major and trace element data for NIST SRM 610 and NIST SRM 612 glass reference materials. Geostandards Newslett. 21, 115–144.
Peters, T., 1968. Distribution of Mg, Fe, Al, Ca, and Na in coexisting olivine, orthopyroxene and clinopyroxene in the Totalp serpentinite (Dravos, Switzerland) and in alpine metamorphosed Malenco serpentinite (N. Italy). Contrib. Miner. Petrol. 18, 65–75.
Pettersen, K., 1883. Sagvandite, en ny bergart. Tromsö Mus. Aarshefter 6, 81.
Pinsent, R.H., Hirst, D.M., 1977. The metamorphism of the Blue River ultramafic body, Cassiar, British Columbia, Canada. J. Petrol. 18, 567–594.
Pitcairn, I., Boskabadi, A., Broman, C., Boyce, A., Teagle, D., Cooper, M., Azer, M., Mohamed, F., Stern, R., 2013. Regional carbonate alteration in the eastern desert of Egypt: isotopic evidence for a mantle-derived fluid source. Geophys. Res. Abstracts 15, EGU2013-9967.
Quick, J.E., 1990. Geology and origin of late Proterozoic Darb Zubaydah ophiolite, Kingdom of Saudi Arabia. Geol. Soc. Am. Bull. 102, 1007–1020.
Ramadan, T.M., Abdelsalam, M.G., Stern, R.J., 2001. Mapping gold bearing massive sulfide deposits in the Neoproterozoic Allaqi suture, southeast Egypt with Landsat TM and SIR-C/X-SAR images. Photogr. Eng. Remote Sens. 67, 491–497.

Randall, B., 1960. Sagvandites of Lyngen, Troms, North Norway. XXI International Geological Congress (Norden) VIII, pp. 443–451.
Raymond, L.A., 2002. The Study of Igneous, Sedimentary and Metamorphic Rocks. McGraw-Hill, Boston, pp. 720.
Reitan, P., Geul, J., 1958. On the formation of carbonate bearing ultrabasic rock at Kviteberg, Lyngen, Northern Norway. Nor. Geol. Unders. 205, 111–127.
Ren, D., Abdelsalam, M.G., 2006. Tracing along-strike structural continuity in the Neoproterozoic Allaqi-Heiani suture, southeastern Egypt using principal component analysis (PCA), fast Fourier transformation (FFT), and redundant wavelet transformation (RWT) of ASTER data. J. Afr. Earth Sc. 44, 181–195.
Richardson, S.W., Gilbert, M.C., Bell, P.M., 1969. Experimental determination of kyanite–andalusite and andalusite–sillimanite equilibria; the aluminum silicate triple point. Am. J. Sci. 267, 259–272.
Rosenbusch, H., 1884. Über den Sagvandite. Neues Jahrb. Mineral., Abh. 1, 195.
Rudnick, R.L., McDonough, W.F., Chappell, B.W., 1993. Carbonatite metasomatism in the northern Tanzanian mantle: petrographic and geochemical characteristics. Earth Planet. Sci. Lett. 114, 463–475.
Schreyer, W., Ohnmacht, W., Mannchen, J., 1972. Carbonate-orthopyroxenites (sagvandites) from Troms, northern Norway. Lithos 5, 345–364.
Seifritz, W., 1990. CO_2 disposal by means of silicates. Nature 345, 486.
Stern, R.J., Gwinn, C.J., 1990. Origin of Late Precambrian intrusive carbonates, eastern Desert of Egypt and Sudan: C, O and Sr isotopic evidence. Precambr. Res. 46, 259–272.
Stern, R.J., Kröner, A., Manton, W.I., Reischmann, T., Mansour, M., Hussein, I., 1989. Geochronology of the late Precambrian Hamisana Shear zone, Red Sea Hills, Sudan and Egypt. J. Geol. Soc. 146, 1017–1030.
Stern, R.J., Nielsen, K.C., Best, E., Sultan, M., Arvidson, R.E., Kröner, A., 1990. Orientation of late Precambrian sutures in the Arabian-Nubian shield. Geology 18, 1103–1106.
Takahashi, E., 1987. Origin of basaltic magmas–implications from peridotite melting experiments and an olivine fractionation model. Bull. Volcanol. Soc. Jpn., 2nd Ser. 30, S17–S40.
Trommsdorff, V., Evans, B.W., 1974. Alpine metamorphism of peridotitic rocks. Schweiz. Mineral. Petrogr. Mitt. 54, 333–352.
Trommsdorff, V., López Sánchez-Vizcaíno, V., Gómez-Pugnaire, M.T., Müntener, O., 1998. High pressure breakdown of antigorite to spinifex-textured olivine and orthopyroxene, SE Spain. Contrib. Miner. Petrol. 132, 139–148.
Uçurum, A., 2000. Listwaenites in Turkey: perspectives on formation and precious metal concentration with reference to occurrences in East-Central Anatolia. Ofioliti 25, 15–29.
Vakanjak, B., Petrovic, B., Tomanec, R., Starostin, V., 1984. The hydrothermal metamorphic formation of vein magnesite deposits associated with ultramafic complexes. Int. Geol. Rev. 26, 673–689.
Vance, J.A., Dungan, M.A., 1977. Formation of peridotites by deserpentinization in the Darlington and Sultan areas, Cascade Mountains, Washington. Geol. Soc. Am. Bull. 88, 1497–1508.
Veizer, J., Hoefs, J., Ridler, R.H., Jensen, L.S., Lowe, D.R., 1989. Geochemistry of Precambrian carbonates: I. Archean hydrothermal systems. Geochim. Cosmochim. Acta 53, 845–857.
White, R.W., 1966. Ultramafic inclusions in basaltic rocks from Hawaii. Contrib. Miner. Petrol. 12, 245–315.
Zoheir, B.A., Klemm, D.D., 2007. The tectono-metamorphic evolution of the central part of the Neoproterozoic Allaqi-Heiani suture, South Eastern Desert of Egypt. Gondwana Res. 12, 289–304.